Ultrafast ZnO nanowire lasers: nanoplasmonic acceleration of gain dynamics at the surface plasmon polariton frequency

Themistoklis P. H. Sidiropoulos[1*], Robert Röder[2], Sebastian Geburt[2], Ortwin Hess[1], Stefan A. Maier[1], Carsten Ronning[2], and Rupert F. Oulton[1*]

1. Imperial College London, Prince Consort Road, UK-SW7 2BZ London, United Kingdom

2. University of Jena, Max-Wien-Platz 1, D-07743 Jena, Germany

**Contact: r.oulton@imperial.ac.uk and t.sidiropoulos10@imperial.ac.uk*

Light-matter interactions are inherently slow as the wavelengths of optical and electronic states differ greatly. Surface plasmon polaritons, electromagnetic excitations at metal-dielectric interfaces, have generated significant interest because their spatial scale is decoupled from the vacuum wavelength, promising accelerated light-matter interactions. Meanwhile, the possibility of accelerated dynamics in recently demonstrated surface plasmon lasers remains to be verified. In this letter, we report the observation of <800 fs pulses from hybrid plasmonic zinc oxide (ZnO) nanowire lasers. Operating at room temperature, ZnO excitons lie near the SPP frequency in such silver-based plasmonic lasers, leading to accelerated spontaneous recombination, gain switching, and gain recovery compared to conventional ZnO nanowire lasers. Surprisingly the laser dyanmics can be as fast as gain thermalization in ZnO, which precludes lasing in the thinnest nanowires (diameter < 120 nm). The capability to combine surface plasmon localization with ultrafast amplification provides the means for generating extremely intense optical fields with applications in sensing, non-linear optical switching, as well as in the physics of strong field phenomena.

Lasers that use metallic cavities have emerged recently as a new class of light source[1–3]. *Plasmonic lasers* achieve optical confinement and feedback using surface plasmon polaritons (SPPs), quasi-particles of photons and electrons at metal-dielectric interfaces, which can be amplified by suitable optical gain media[4]. The high gain of inorganic crystalline semiconductors is typically necessary to overcome fast electron scattering in metals ($\sim$10 fs), which leaves plasmonic lasers with high parasitic cavity loss. Nevertheless, SPPs offer the capability to reduce optical mode sizes far below the scale of the vacuum wavelength[3,5–8] leading to compact lasers that can generate extremely focussed optical excitations on potentially ultrafast time scales[1,9] with applications in Raman sensing[10–12], non-linear frequency generation[13–15], and non-linear optical switching[16]. Despite the draw-back of loss, numerous plasmonic lasers have been reported recently with progress being made towards reducing the laser threshold to a point where practical applications are viable. In particular, several devices now operate at room temperature[7,17] and even under electrical injection[18]. While the practical issues of these devices have seen progress, few experimental works have studied their underlying limitations and capabilities. In terms of limitations, it is currently unclear how much confinement is realistically sustainable. In plasmonics confinement is associated

with loss and accelerated recombination, which both affect laser threshold[19–21]. In particular, only a few works have reported plasmonic laser action near the SP frequency where the electromagnetic field equally shares energy with electron polarization maximizing both confinement and loss[6]. As for capabilities, the expectation that plasmonic lasers are ultrafast amplifiers[9,19,22] due to optical confinement and the corresponding Purcell effect[23–25], has yet to be experimentally proven. Certainly, accelerated gain dynamics are achievable[26] since the Purcell effect accelerates both spontaneous and stimulated recombination rates due to the intrinsic relationship between Einstein's A and B coefficients. However, it is less clear what degree of accelerated recombination is sustainable due the effect on threshold and the finite time scale of carrier thermalization in the amplifying medium. In this article we address both of these questions. Firstly, we report the demonstration of hybrid plasmonic[27] lasers at room temperature operating near the SPP frequency by exploiting the ultraviolet gain spectrum of ZnO nanowires. Secondly, we report accelerated laser dynamics of plasmonic lasers compared to conventional *photonic* ZnO nanowire lasers. Remarkably, we have measured sub-picosecond plasmonic lasers pulses, within the ultrafast regime, where temporal dynamics are generally only accessible by non-linear all-optical techniques[28]. Here we have used a novel double-pump approach that exploits the non-linearity of the laser process to expose its own dynamics.

The plasmonic lasers under investigation consist of individual ZnO nanowires placed on a 10 nm thick lithium fluoride (LiF) spacer layer over a silver (Ag) substrate, as shown in Fig. 1a. The insulating spacer layer affords optical confinement control and isolates ZnO excitations from quenching at the metal surface[5]. The *photonic* lasers consist of ZnO nanowires from the same batch of nanowires but placed on a Si/SiO_2 substrate[29]. The finite length of each nanowire ($5 < L < 20$ m) defines a cavity; laterally confined modes propagate backwards and forwards along the nanowire with feedback arising from modal reflection at the end-facets. Under optical pumping, ZnO is capable of the extremely strong optical gain necessary to achieve plasmonic lasing near its bandedge at 3.37 eV. This originates mainly from the two lowest energy of three excitons ($\hbar\omega_A = 3.309$ eV, $\hbar\omega_B = 3.315$ eV and $\hbar\omega_C = 3.355$ eV) that have a sufficiently large binding energy (60 meV) to be stable at room temperature[30] (Fig. 1b). Under weak optical pumping, spontaneous photoluminescence and gain occur below the band-edge near 3.24 eV through either exciton-exciton scattering or via optical phonon scattering ($\hbar\omega_{LO} = 72$ meV)[31,32]. Meanwhile, under strong excitation above the Mott density, carrier screening causes exciton dissociation into an electron hole plasma (EHP), which together with band-gap renormalization, provides gain as far below the band-edge as ~3.19 eV[33]. Even for photonic nanowire lasers, the EHP mechanism is required for sufficient gain to overcome the high cavity loss[34,35]. Thus, we also expect the EHP mechanism to occur in plasmonic lasers.

The dispersion relations for the transverse modes of the plasmonic and photonic devices are both influenced by the excitonic dispersion of ZnO. Figure 1b shows the dispersion relation of the fundamental plasmonic transverse mode for a nanowire diameter of $D = 130$ nm. Since the SPP frequencies of Silver-Air ($\hbar\omega_{SP}^{air} = 3.65$ eV) and Silver-ZnO ($\hbar\omega_{SP}^{ZnO} = 2.90$ eV) encompass the exciton energies of ZnO, excitons should couple strongly to SPPs (Fig. 1b). Indeed, calculations show a surface plasmon frequency within the absorption spectrum of ZnO, where we have used a Brendel-Bormann model for the permittivity of silver, which was fit to the data of Palik[36,37]. The large surface plasmon wavenumber within ZnO's gain spectrum suggests that strong optical mode confinement occurs (see supplementary information). In previous plasmonic laser work, a hybrid plasmonic mode[27], shown in Fig. 1c, was identified through the absence of a mode cut-off and the enhancement of spontaneous recombination[5]. In contrast, a photonic nanowire of $D = 150$ nm is very close to cut-off within ZnO's gain spectrum. Indeed, previous works have not observed photonic ZnO nanowire lasers for $D < 150$ nm[29]. Both plasmonic and photonic laser can also support other transverse modes for thicker nanowires, but these generally exhibit weaker confinement and feedback (supplementary information)[29]. To our knowledge, all reported photonic ZnO lasers have operated via the EHP mechanism with emission energies near 3.23 eV where polariton dispersion is relatively weak[35]. In contrast, the plasmonic lasers in this work operate in the vicinity of the exciton energies, near 3.30 eV.

Each nanowire was optically pumped at a wavelength of 355 nm with nominally 150 fs pulses at a repetition rate of 800 kHz, chosen to avoid heating in the devices, but also to probe their ultrafast dynamics. The spectra shown in Fig. 2a are representative of photonic and plasmonic lasers pumped at twice their respective threshold energy densities (inset of Fig. 2a). In general, plasmonic lasers show a suppressed super-linear light vs pump response near the laser transition compared to photonic devices, which is characteristic of enhanced spontaneous recombination arising from mode localization and reduced mode competition[2]. (Other examples of plasmonic lasers are shown in the supplementary information). The difference in thresholds of 43 Jcm^{-2} and 200 J cm^{-2} for the photonic and plasmonic laser, respectively, are reminiscent of the differences observed in previous work[5]. The role of SPPs in the plasmonic lasers can also be clearly confirmed in their emission polarisation: plasmonic lasers are polarized along the nanowire, which is consistent with the dominant field components of hybrid SPP modes[27], as shown in Fig. 2a. Above threshold photonic devices lase in the EHP regime between $3.19 - 3.25$ eV while plasmonic devices only lase above 3.25 eV (Fig. 2b). The blue shift occurs as the lossy plasmonic cavity requires considerably higher gain, which can only be achieved nearer the exciton transition energies[38]. Moreover, a reduction in nanowire diameter causes a further blue shift, even beyond the energies of the A and B excitons,

primarily due to higher loss for smaller diameter nanowires, but also due to state filling[39]. The threshold behaviour, high gain and the laser mode polarisation strongly suggest the role of SPP modes in the lasing action. Furthermore, we have measured plasmonic lasers with diameters down to $D = 120$ nm where photonic lasing cannot occur[29]. Remarkably, we do not observe a significant increase in plasmonic laser threshold with decreasing diameter, despite the apparent increases in loss (supplementary information).

The stark differences between plasmonic and photonic light vs pump curves and spectral responses suggest a modification of the laser process that both accelerates and redistributes spontaneous recombination[2]. In order to examine the influence of confinement on stimulated emission dynamics, ideally we should measure the temporal shape of light pulses emanating from these lasers. This presents a significant challenge as plasmonic lasers are anticipated to operate in the sub picosecond regime, which is at the limit of electrical detection techniques, such as streak cameras[26]. Generally, non-linear all-optical techniques would be required[28] to characterize such short light pulses, however, individual nanowires produce insufficient signal for such time resolved non-linear spectroscopies. Here, we have explored the temporal dynamics of these nanowire-based lasers by measuring their response to optical excitation with two energetically identical pump pulses separated by a variable time delay, τ. The technique uses the inherent non-linearity of the population inversion to reveal internal temporal dynamics that establishes clear bounds on the characteristic laser response times.

Figure 3 illustrates the expected response of a hypothetical laser cavity incorporating a 3-level electronic gain system to the double-pump pulse strategy (Methods). Here, the intensity of one beam is sufficient to excite the laser, whereas the second beam is weaker and cannot induce lasing on its own. The laser's response as a function of time delay indicates spontaneous recombination and gain recovery dynamics of the laser. The chosen parameters reproduce the observed responses of the measured plasmonic lasers.

For $\tau < 0$ the weak pulse initially excites carriers into the upper level, which rapidly thermalize to the excited state and subsequently recombine spontaneously (Fig. 3a). This population is then further excited by the strong pulse causing the system to lase. Prior to the arrival of the strong pulse the excited state population exponentially decays at the spontaneous recombination rate, thus increasing the laser output power with decreasing delay between the pulses, as shown in Fig. 3c. Around the zero delay point we can expect intricate interference of the two input pulses[40], which only becomes apparent with varying time delay, as shown in Fig. 3c. For $\tau > 0$ the strong pump pulse initially creates an inversion, generating an output laser pulse that partially depletes the excited

state population (Fig. 3b). The weak pump pulse may now have a significant effect on the laser's response as the residual excited state population can facilitate lasing.

For $\tau > 0$ we can further identify three situations. For a small time delay the excited state is still near peak population and the weak pump pulse merely amplifies the output pulse. Note that the strong pump pulse depletes the ground state and thus reduces the nanowire's absorption of the weaker pump pulse. For increased time delays, absorption of the weaker pump pulse grows and this leads to the gradual formation of a second output pulse as well as the amplification of the first output pulse, as shown in Fig. 3b. The two output pulses emerge on distinct time scales: time delays between pump and output pulses, t_1 and t_2, occur for the strong and weak pump pulses, respectively; and the peak to peak separation of the two output pulses is τ_m. These time scales are related to the pump pulse delay by $\tau_m = \tau - (t_1 - t_2)$. Note that since the initial pump pulse must create the inversion, usually $t_1 \gg t_2$. The double pump response reaches a maximum, denoted by t_{max}, when the absorption of the second pump pulse recovers also marking the termination of the first output pulse (Fig. 3c). Finally, for large time delays the residual excited population gradually depletes with the spontaneous recombination time until a point where the second pump pulse no longer induces lasing and merely creates incoherent emission.

This simple theoretical model predicts a number of characteristics that agree well with the measured double-pump responses of the plasmonic and photonics lasers, shown in Fig. 4. To make a fair comparison of the two devices, we chose similar normalized pump energy densities ranging between once and twice the respective threshold values (Fig. 4c,d). Furthermore, since the responses are non-linear, we also fixed the power ratio of the two pump pulses at 1/5th. The plasmonic laser clearly shows accelerated spontaneous recombination, evident from the steeper exponential decay for $\tau < 0$ compared with the photonic device. A quantitative assessment of the Purcell factor is difficult since the photonic laser has an almost flat response for $\tau < 0$ and the plasmonic laser exhibits a shallower non-linear light versus pump response than the photonic device, as shown in Figs. 4c and 4d, respectively. The magnitude of the enhanced spontaneous recombination in the plasmonic device is clearer for $\tau > 0$, where after-pulsing from the weaker pump pulse persists for less than a 10th of the time scale with respect to the photonic device. Interestingly, the double pump responses in Figs. 4a and 4b become faster with decreasing pump energy density, which is counterintuitive. The reader should note that both pump pulses change intensity here: since the ratio of pump intensities is fixed at 1/5th, a second output pulse becomes less sustainable for larger time delays, leading to an apparently faster double-pump response. A more reliable indication of the accelerated plasmonic laser dynamics is the peak response time, t_{max}. While the observed decay

relates to light-matter interaction processes, t_{max} indicates the termination of the first output pulse. Remarkably, the plasmonic laser reaches t_{max} much earlier than the photonic device. This places an upper limit on the first output pulse width of the plasmonic lasers at < 1.9 ps, whereas the photonic laser's pulse width has an upper limit in the region of < 12.5 ps.

In order to expose the laser pulse dynamics in more detail, we have resolved the laser output spectrally as well as temporally. In this way, we can access information related to the spectral phase of the two output pulses, which carries temporal information[28]. According to our model, we expect to observe the interference of two output pulses separated by a time delay, τ_m, as shown in Fig. 3b, which we represent by two time dependant electric field amplitudes $\mathcal{E}_1(t;\tau)$ and $\mathcal{E}_2(t-\tau_m;\tau)$. Since we resolve the time averaged interference of these two pulses in our spectrometer, we expect a modulation of the spectral intensity of the form,

$$\Delta I(\omega;\tau) = 2E_1(\omega;\tau)E_2(\omega;\tau)\cos\big(\omega\tau_m + \Delta\phi(\omega;\tau)\big) \quad (1)$$

where $\Delta\phi(\omega;\tau) = \phi_1(\omega;\tau) - \phi_2(\omega;\tau)$ is the difference between the spectral phases of the two pulses. Indeed, Eq. (1) describes the observed modulated double pump spectra, shown in Fig. 5a. Specifically, with increasing delay, τ, we see a decrease in the period of sinusoidal modulation, which also shifts with τ indicating the temporal broadening of one pulse with respect to the other. This is consistent with the interference of two output pulses, where the second pulse broadens in time for increasing time delay, τ. Remarkably, when these data are transformed to the time domain (Fig. 5b) we recover sidebands following a linear trend, which we attribute to the relationship between pump and output pulse delays, $\tau_m = \tau - (t_1 - t_2)$ (see Fig. 3b). From simulations, we know that $t_1 \gg t_2$, and so $t_1 \approx \tau_{on}$, which is the time taken to establish the first output pulse. Here, we observe a $\tau_{on} \approx 1.1$ ps which is determined by the thermalization of the EHP[41]. Since EHP thermalization is solely dependent on the gain material, we expect τ_{on} to be independent of the electromagnetic environment (see Fig. 6).

The measured sideband signal is proportional to a modified temporal convolution of the two output pulses, as shown in Eq. (2). While this convolution restricts explicit temporal pulse re-construction for each time delay, τ, it does indicate the relative strengths of the two output pulses as a function of τ.

$$\Gamma(t > 0;\tau) = \mathcal{F}^{-1}\{\Delta I(\omega;\tau)\} = \mathcal{E}_1(-t;\tau) * \mathcal{E}_2(t-\tau_m;\tau) \quad (2)$$

Figure 5b, showing the Fourier transformed spectral response versus time delay, now clearly highlights the three regimes identified above. For $\tau \gtrsim 0$, no interference is visible indicating that

only one output pulse is formed and all additional power from the weaker pump pulses simply adds to the first output pulse. With increasing delay we eventually observe the formation of a second output pulse at $\tau_{on} = 1.1$ps. For $\tau_{on} \leq \tau \leq t_{max}$, the second output pulse forms and competes with the first pulse for gain. This is evident from the modulation visibility's bi-exponential decay with delay τ (inset of Fig. 5b). The initial decay is faster as two output pulses compete for gain, whereas the slower decay corresponds only to the second pulse's use of residual excited carriers, $\tau > t_{max}$, which is indicative of the EHP recombination time[31]. We emphasize that the transition from fast to slow decay corresponds directly to the maximum in the double-pump response, $\tau = t_{max}$, observed in Fig. 4, where the second output pulse starts to dominate over the first. Since $\tau_{on} \approx t_1$ indicates the start of the first output pulse and t_{max} indicates where it terminates, their difference, $t_{max} - \tau_{on}$, suggests this plasmonic laser has a pulse width of $\sim$800 fs.

These two lasers show clear differences, but it is also remarkable that these trends are seen in the vast majority of measured devices. Moreover, we have measured the temporal responses of a number of nanowire lasers with diameters near the cut-off diameter of photonic devices, as shown in Fig. 6a. The effect of SPP confinement becomes all the more apparent as we see acceleration of the optical processes with decreasing nanowire diameter. In contrast, the photonic devices become slower with decreasing diameter, which we attribute to the loss of mode confinement. Perhaps the most remarkable difference between the plasmonic and photonic devices is the time at which the second output pulse is maximized, shown in Fig. 6b. On average $t_{max} \approx 1.6$ ps is consistently faster for plasmonic lasers and given that $\tau_{on} \approx 1$ ps suggests sub-ps pulse widths. The difference, $t_{max} - \tau_{on}$, for photonic lasers suggest much broader output pulses. The pulse widths of 4-5 ps for $D < 200$ nm are consistent with the EHP decay time for ZnO[31]. Interestingly for larger photonic nanowire diameters, a change in output polarization indicates that a different transverse mode lases, and the value of t_{max} suggests a different gain mechanism to the EHP one occurs, which should be explored in future work. Meanwhile plasmonic lasers clearly operate on a sub-ps timescale and could be potentially even faster only limited by the EHP formation time.

In this work, we used ZnO as gain material to demonstrate plasmonic laser devices operating close to the surface plasmon frequency. A spectral comparison with photonic devices verified that these metal based devices have plasmonic character and operate at blue-shifted energies. Furthermore, by using a novel double-pump approach, based on the nonlinearity of the lasing process itself, we verified the anticipated ultrafast plasmonic laser dynamics in the sub-1ps regime. While plasmonic lasers become faster with decreasing nanowire diameter due to the electromagnetic environment, the time taken to establish laser action is material dependent and remains constant. This suggests

that recombination in plasmonic devices could potentially be too fast to allow the build-up of a population inversion[20]. This is one argument for why no plasmonic lasing was observed in sub 120 nm diameter wires in our study. We note that other authors have reported lasing away from the SP frequency in nanowires with diameters < 60 nm at low temperature[3,5]. While there is considerable scope for ultrafast plasmonic lasers, these devices are ultimately limited by internal relaxation processes of the chosen gain medium that cannot be engineered by the Purcell effect.

Methods

Sample preparation

To construct the plasmonic laser, we thermally evaporated 100 nm Ag and then 10 nm of LiF on a Si substrate. The nanowires were dry transferred from the substrate onto the evaporated sample by bringing the surfaces in contact and slightly moving the nanowire substrate horizontally against the sample. The same technique was used to transfer nanowires onto the Si/SiO_2 (1.5µm thermal oxide) to construct photonic laser samples. While the substrate materials of the two devices were chosen for practical reasons, the different refractive indices do not influence optical mode confinement as the nanowires are predominantly embedded in air[29]. Due to the mechanical deposition approach, thinner nanowires also tended to be shorter, but all nanowires had lengths in the range $5 < L < 20\ \mu$m. The nanowires themselves were fabricated with the VLS technique described in Ref.[29]. The nanowire diameters typically vary, $100 < D < 300$ nm. Variations in the measured temporal responses were observed for different batches of nanowires, so the reported data set is for nanowire lasers from the same growth batch. Spectral characteristics were consistent between batches.

Optical set-up

To measure the temporal response, we sent about 45% of the incoming pump beam through a delay line and combined both beams again using a half-mirror (see schematic in supplementary information). The two pump beams are then focussed through a cylindrical lens (f = 300 mm) and a UV microscope objective (20x NA=0.4) onto the sample to form two overlapping elliptical beams that completely encompass a single nanowire. Prior to characterising the temporal dynamics of an individual nanowire laser we first investigate its operation under excitation by a single pulse.

To measure the spectral-temporal lasing response near $\tau \approx 0$ we detect nanowire emission in a spectrometer (Princeton instruments SP2300). The spectrometer's resolution of ~0.14 nm allows us to measure time delays on the order of τ_m = 4 ps, where the expected spectral interference period is ~0.12 nm.

To measure the spectrally integrated temporal response of our devices we modulate the weak pump pulse and detect the time integrated modulated signal amplitude of a photo diode with a Lock-In amplifier (Stanford Research Systems SRS830).

Simulation of lasing and temporal response

The integrated emission spectrum against the pump power was fitted to Casperson's model[41] with a single fitting parameter, x_0. Here, for the photonic wires we usually obtain $x_0 \ll 0.1$ and for the

plasmonic wires $x_0 > 0.1$, which indicates a high spontaneous emission factor for the plasmonic devices.

To model the dynamics of the plasmonic lasers we use a simple 3-level laser rate equation model. This approximation is valid provided carrier de-phasing (<100 fs) is much faster than the response time of the laser, which is the case here since the time taken to establish lasing is on the order of ~ 1 ps. The rate equations are,

$$\dot{N}_3 = RN_1 - N_3/\tau_{therm} \quad (3)$$

$$\dot{N}_2 = -\beta F A_0 s(N_2 - N_1) - FA_0 N_2 + N_3/\tau_{therm} \quad (4)$$

$$\dot{s} = \beta F A_0 s(N_2 - N_1) + \beta F A_0 N_2 - \gamma s \quad (5)$$

Here, N_i is the population of the ith state with a maximum of $N_T = 10^6$, $\beta = 0.2$ is the spontaneous emission factor, $A_0^{-1} = \tau_m = 350$ ps is the ZnO exciton lifetime[42], $F = 10$ is the Purcell factor, R is the input pump rate, s is the photon cavity number, and $\gamma^{-1} = 50$ fs is the cavity photon lifetime, and $\tau_{therm} = 0.5$ ps is the thermalization time. Clearly, this simplified rate equation model cannot describe all gain processes occurring in the semiconductor such as the EHP formation. Therefore, the time scales shown in Fig. 3 are just an indication of the temporal processes occurring. The parameters for the rate equation model were chosen so that the calculated double pump response qualitatively matches experimental observations. We note that this underestimates the time taken to establish lasing. Further investigations based on spatio-temporal many-body semiconductor laser theory[44] are a subject for future studies. The double-pump pulses separated by a time delay, τ, are described by a pump rate, $R(t) = R_0(P(t) + \rho P(t-\tau) + 2\rho P(t)^2 \cos(\omega\tau))$, where ρ is the ratio of the two peak pulse powers and $P(t-\tau) = \exp(-(t-\tau)^2 \ln 2/\sqrt{2}t_{pulse}^2)$. Although the pump laser produces pulses of ~ 150 fs at a wavelength of 355 nm, we have modelled the dynamics using a pulse width of $t_{pulse} = 250$ fs to account for the dispersion of the optics in the measurement apparatus.

References

1. Bergman, D. & Stockman, M. Surface Plasmon Amplification by Stimulated Emission of Radiation: Quantum Generation of Coherent Surface Plasmons in Nanosystems. *Phys. Rev. Lett.* **90,** 1–4 (2003).
2. Ma, R., Oulton, R. F., Sorger, V. J. & Zhang, X. Plasmon lasers: coherent light source at molecular scales. *Laser Photonics Rev.* **7,** 1–21 (2012).
3. Lu, Y.-J. *et al.* Plasmonic nanolaser using epitaxially grown silver film. *Science* **337,** 450–3 (2012).
4. Oulton, R. F. Surface plasmon lasers: sources of nanoscopic light. *Mater. Today* **15,** 592–600 (2012).
5. Oulton, R. F. *et al.* Plasmon lasers at deep subwavelength scale. *Nature* **461,** 629–632 (2009).
6. Noginov, M. A. *et al.* Demonstration of a spaser-based nanolaser. *Nature* **460,** 1110–1112 (2009).
7. Ma, R., Oulton, R. F., Sorger, V. J., Bartal, G. & Zhang, X. Room-temperature sub-diffraction-limited plasmon laser by total internal reflection. *Nat. Mater.* **10,** 110–113 (2010).
8. Hill, M. T. *et al.* Lasing in metal-insulator-metal sub-wavelength plasmonic waveguides. *Opt. Express* **17,** 11107–11112 (2009).
9. Stockman, M. I. The spaser as a nanoscale quantum generator and ultrafast amplifier. *J. Opt.* **12,** 024004 (2010).
10. Kneipp, K. *et al.* Single Molecule Detection Using Surface-Enhanced Raman Scattering (SERS). *Phys. Rev. Lett.* **78,** 1667–1670 (1997).
11. Nie, S. Probing Single Molecules and Single Nanoparticles by Surface-Enhanced Raman Scattering. *Science* **275,** 1102–1106 (1997).
12. Anker, J., Hall, W., Lyandres, O. & Shah, N. Biosensing with plasmonic nanosensors. *Nat. Mater.* **7,** 442–453 (2008).
13. Danckwerts, M. & Novotny, L. Optical Frequency Mixing at Coupled Gold Nanoparticles. *Phys. Rev. Lett.* **98,** 026104 (2007).
14. Aouani, H., Rahmani, M., Navarro-Cía, M. & Maier, S. A. Third-harmonic-upconversion enhancement from a single semiconductor nanoparticle coupled to a plasmonic antenna. *Nat. Nanotechnol.* **9,** 290–294 (2014).
15. Kim, S. *et al.* High-harmonic generation by resonant plasmon field enhancement. *Nature* **453,** 757–760 (2008).
16. Yu, Z., Veronis, G., Fan, S. & Brongersma, M. L. Gain-induced switching in metal-dielectric-metal plasmonic waveguides. *Appl. Phys. Lett.* **92,** 041117 (2008).
17. Khajavikhan, M. *et al.* Thresholdless nanoscale coaxial lasers. *Nature* **482,** 204–207 (2012).
18. Ding, K. *et al.* Room-temperature continuous wave lasing in deep-subwavelength metallic cavities under electrical injection. *Phys. Rev. B* **85,** 041301 (2012).
19. Khurgin, J. B. & Sun, G. Comparative analysis of spasers, vertical-cavity surface-emitting lasers and surface-plasmon-emitting diodes. *Nat. Photonics* **8,** 468–473 (2014).
20. Khurgin, J. B. & Sun, G. Scaling of losses with size and wavelength in nanoplasmonics and metamaterials. *Appl. Phys. Lett.* **99,** 211106 (2011).
21. Khurgin, J. B. & Sun, G. Injection pumped single mode surface plasmon generators: threshold, linewidth, and coherence. *Opt. Express* **20,** 15309–15325 (2012).
22. Wuestner, S. *et al.* Control and dynamic competition of bright and dark lasing states in active nanoplasmonic metamaterials. *Phys. Rev. B* **85,** 201406 (2012).
23. Kinkhabwala, A. *et al.* Large single-molecule fluorescence enhancements produced by a bowtie nanoantenna. *Nat. Photonics* **3,** 654–657 (2009).
24. Sorger, V. J. *et al.* Strong Molecular Fluorescence inside a Nanoscale Waveguide Gap. *Nano Lett.* **11,** 4907–4911 (2011).
25. Russell, K., Liu, T., Cui, S. & Hu, E. Large spontaneous emission enhancement in plasmonic nanocavities. *Nat. Photonics* **6,** 459–462 (2012).

26. Altug, H., Englund, D. & Vučković, J. Ultrafast photonic crystal nanocavity laser. *Nat. Phys.* **2,** 484–488 (2006).
27. Oulton, R. F., Sorger, V. J., Genov, D. A., Pile, D. F. P. & Zhang, X. A hybrid plasmonic waveguide for subwavelength confinement and long-range propagation. *Nat. Photonics* **2,** 496–500 (2008).
28. Trebino, R. Measuring the seemingly immeasurable. *Nat. Photonics* **5,** 189–192 (2011).
29. Zimmler, M. A., Capasso, F., Müller, S. & Ronning, C. Optically pumped nanowire lasers: invited review. *Semicond. Sci. Technol.* **25,** 024001 (2010).
30. Yoshikawa, H. & Adachi, S. Optical constants of ZnO. *Jpn. J. Appl. Phys.* **36,** 6237–6243 (1997).
31. Shih, T., Mazur, E., Richters, J.-P., Gutowski, J. & Voss, T. Ultrafast exciton dynamics in ZnO: Excitonic versus electron-hole plasma lasing. *J. Appl. Phys.* **109,** 043504 (2011).
32. Klingshirn, C. ZnO: material, physics and applications. *ChemPhys Chem* **8,** 782–803 (2007).
33. Röder, R. *et al.* Continuous Wave Nanowire Lasing. *Nano Lett.* **13,** 3602–3606 (2013).
34. Zimmler, M. A., Bao, J., Capasso, F., Müller, S. & Ronning, C. Laser action in nanowires: Observation of the transition from amplified spontaneous emission to laser oscillation. *Appl. Phys. Lett.* **93,** 051101 (2008).
35. Versteegh, M. A. M., Vanmaekelbergh, D. & Dijkhuis, J. I. Room-Temperature Laser Emission of ZnO Nanowires Explained by Many-Body Theory. *Phys. Rev. Lett.* **108,** 157402 (2012).
36. Rakic, A. D., Djurisic, A. B., Elazar, J. M. & Majewski, M. L. Optical Properties of Metallic Films for Vertical-Cavity Optoelectronic Devices. *Appl. Opt.* **37,** 5271–5283 (1998).
37. Palik, E. D. *Handbook of Optical Constants of Solids, Author and Subject Indices for Volumes I, II, and III*. (Elsevier Science & Technology, 1997).
38. Liu, X., Zhang, Q., Yip, J. N., Xiong, Q. & Sum, T. C. Wavelength Tunable Single Nanowire Lasers Based on Surface Plasmon Polariton Enhanced Burstein–Moss Effect. *Nano Lett.* **13,** 5336–5343 (2013).
39. Klingshirn, C. F. *Semiconductor Optics*. (Springer, 2007).
40. Lebedev, M. V. On the Nature of 'Coherent Artifact'. *J. Exp. Theor. Phys.* **100,** 272–282 (2005).
41. Hendry, E., Koeberg, M. & Bonn, M. Exciton and electron-hole plasma formation dynamics in ZnO. *Phys. Rev. B* **76,** 045214 (2007).
42. Casperson, L. W. Threshold characteristics of multimode laser oscillators. *J. Appl. Phys.* **46,** 5194–5201 (1975).
43. Huang, M. H. *et al.* Room-temperature ultraviolet nanowire nanolasers. *Science* **292,** 1897–9 (2001).
44. Böhringer, K. & Hess, O. A full-time-domain approach to spatio-temporal dynamics of semiconductor lasers. I. Theoretical formulation. *Prog. Quantum Electron.* **32,** 159–246 (2008).

Acknowledgments

This work was sponsored by the UK Engineering and Physical Sciences Research Council (EPSRC) as well as the Deutsche Forschungsgemeinschaft (FOR 1616). R.F.O. is supported by an EPSRC Fellowship (EP/I004343/1) and Marie Curie IRG (PIRG08-GA-2010-277080).

Author contributions

The nanowires where grown by R.R. and S.G.; the simulations were performed by T.P.H.S. and R.F.O.; the experimental measurements were conducted by T.P.H.S.; results were discussed and interpreted by all authors; the manuscript was written by T.P.H.S. and R.F.O. with feedback from all co-authors.

Competing financial interests

The authors declare no competing financial interests.

Figure 1. Sketch of the ZnO plasmonic nanowire laser geometry and its calculated transverse mode characteristics. a Schematic of the geometry and the emission of a ZnO nanowire optically excited with two time-delayed (τ) pump pulses. The inset shows a picture of a lasing plasmonic nanowire. **b** Calculated dispersion relation for various metallic interfaces plotted as photon energy versus normalised momentum (k/k_0). The different curves are for a Silver-Air interface (black dotted line), Silver-ZnO interface (black dashed line), a 150 nm diameter ZnO wire on SiO_2 (pink dash-dotted line) without cut-off k/k_0 < 1.5, and a 130 nm diameter ZnO wire close to a silver surface (pink solid line). The three ZnO exciton lines are labelled with X_a, X_b, X_c and the overlapping shaded areas indicate the EHP gain region (light grey) and plasmonic laser emission region (dark grey). Panels **c** and **d** show calculated nanowire modes for a 130 nm diameter ZnO wire on a Silver/LiF (100/10 nm) interface and a 150 nm diameter ZnO wire on SiO_2 substrate, respectively.

Figure 2. Comparison of measured plasmonic and photonic nanowire laser emission. a Comparison of the measured emission from a selected plasmonic nanowire with a diameter of around 150nm and a thicker ≈ 250nm photonic nanowire on a quartz substrate. The emission is separated into components with polarisation along the nanowire axis (solid curves) and with polarisation perpendicular to the nanowire axis (dashed curves). The inset shows the emitted output power, (P_{out}) normalised to the threshold value ($P_{out}^{(th)}$) against the optical pump energy density (P_{in}); again for the selected plasmonic and photonic nanowire. **b** The measured central emission wavelength of a range of plasmonic nanowires against their diameter. The dashed lines in **a** and **b** labelled X_a, X_b, and X_c represent the ZnO exciton energies.

Figure 3. Numerical simulations of the temporal response under double pump excitation. a, **b** The three panels show the temporal responses of weak and strong pump pulses, the difference in population between excited and ground state (ΔN) normalised to the maximum inversion (N_T), and the normalised cavity photon number (s/s_{max}) for a plasmonic device for two distinct delays $\tau < 0$, and $\tau > 0$, respectively. **c** The left axis shows the simulated output response (P_{out}) to the two pump pulses determined by integrating the cavity photon number at each time delay at and excitation intensity of twice the threshold value, $2P_{in}^{(th)}$ (black solid line). The right axis shows the simulated absorption response of the weak pump pulse modulated by the strong pump pulse to indicate the material's gain depletion and recovery during a plasmonic laser pulse (red dashed line).

Figure 4. Measured temporal response from plasmonic and photonic nanowires under double-pump excitation. a, **b** The total double-pump response of the nanowire lasers (P_{out}) against time delay (τ) for three different pump energy densities of the plasmonic and photonic devices from Fig. 2, respectively. **c**, **d** Laser light-output (P_{out}) versus pump intensity (P_{in}) for the plasmonic and

photonic nanowire both normalized their threshold values ($P_{out}^{(th)}$ and $P_{in}^{(th)}$ respectively). The values for x_0 are obtained by fitting the curves with the model used in Ref.[29]. The vertical arrows (labelled i, ii, and iii) show the strong (solid) and weak (dashed) pump powers used to generate the responses given in **a** and **b**, relative to the lasing curve of each NW. Typically the strong pump pulse is near threshold, $P_{in}^{(th)}$ for situation iii, $1.5 \times P_{in}^{(th)}$ for situation ii, and $2P_{in}^{(th)}$ for situation i.

Figure 5. Measured spectra versus double pump pulse delay for the plasmonic nanowire laser and its Fourier transform. a shows the normalized difference spectrum, $\Delta I(\lambda,\tau)/I_0(\lambda) = I(\lambda,\tau)/I_0(\lambda) - 1$, of the plasmonic nanowire laser for $\tau \geq 0$, where $I(\lambda,\tau)$ is the spectrum under double pump excitation, and $I_0(\lambda)$ is the single strong pump pulse spectrum. The two upper panels show the $\Delta I/I_0$ spectra for the pulse delays, $\tau = 2.1$ ps and $\tau = 3$ ps, indicating the increasing spectral modulation frequency with pulse delay. **b** shows the Fourier transform of each spectrum shown in **a** versus pulse delay. The white trend line follows $t = \tau - \tau_{on} \approx \tau_m$, indicating a turn on time of $\tau_{on} = 1.1$ ps. The inset shows the amplitude decay of the Fourier transformation along the white trend line. The presented data in this figure correspond to measurements at the highest pump power (situation i), shown in Fig. 4**a**.

Figure 6. Comparison of measured characteristic response times in plasmonic and photonic lasers. **a** Comparison of the double pump decay time τ_{i} (see Fig. 4**a**) of different plasmonic (closed circles) and photonic (open circles) nanowire laser, pumped at twice their respective thresholds. The trend of the temporal response with changing nanowire diameter is indicated by the broken lines. Note that photonic lasers exhibit a jump in temporal response due to a change in mode polarisation. In other batches of nanowires, the plasmonic lasers with larger diameters did not exhibit a polarization change. **b** The characteristic temporal parameters τ_{on} (diamonds) and t_{max} (circles) for the same plasmonic (closed symbols) and photonic (open symbols) wires as shown in **a**. The bottom dashed line indicates the average τ_{on}, which is independent of the electromagnetic geometry. The other lines indicate average t_{max} values for the plasmonic and photonic lasers, where the temporal pulse width of each laser can be estimated as $t_{max} - \tau_{on}$.

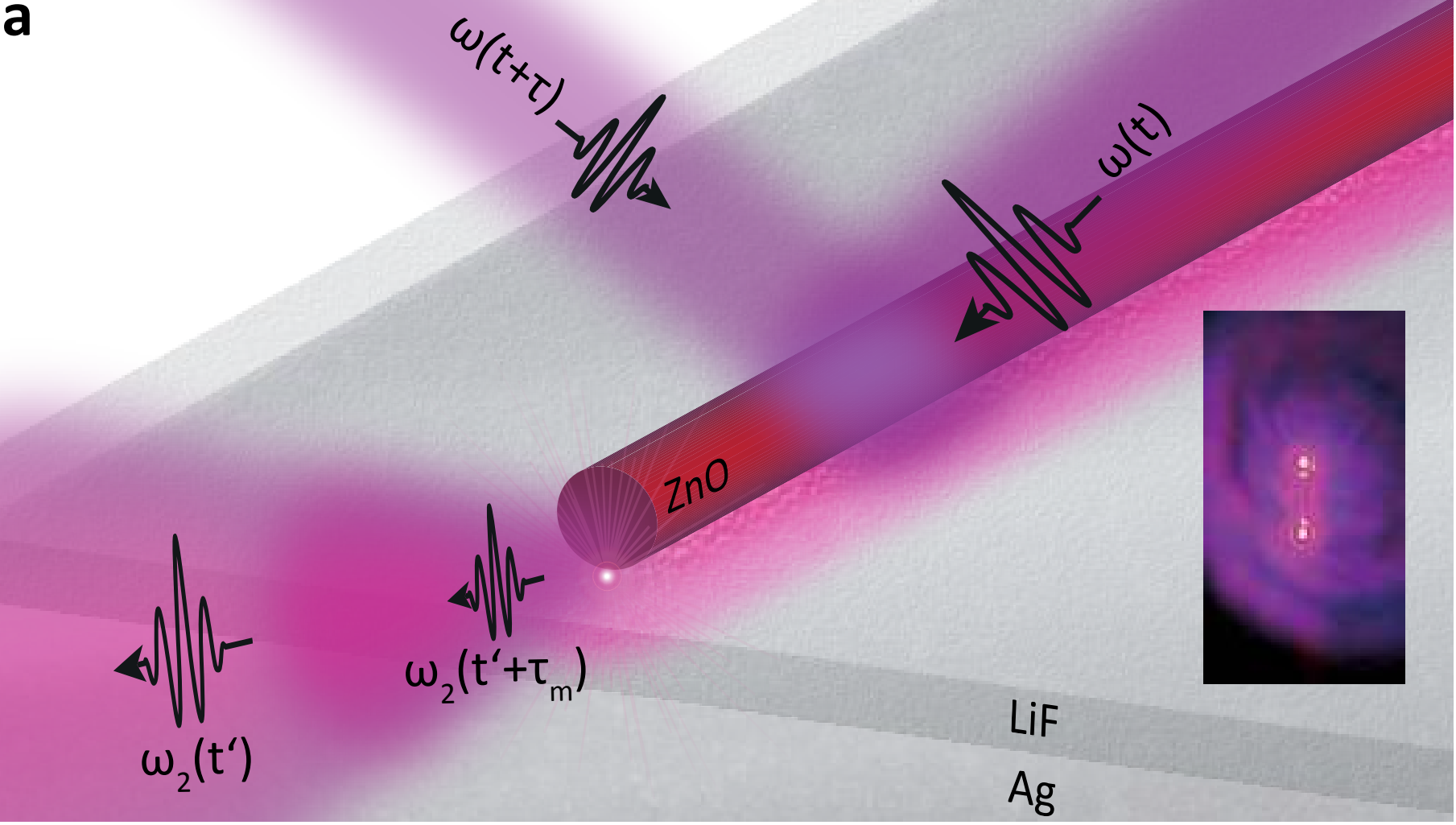
a
ω(t+τ)
ω(t)
ZnO
ω2(t'+τm)
ω2(t')
LiF
Ag

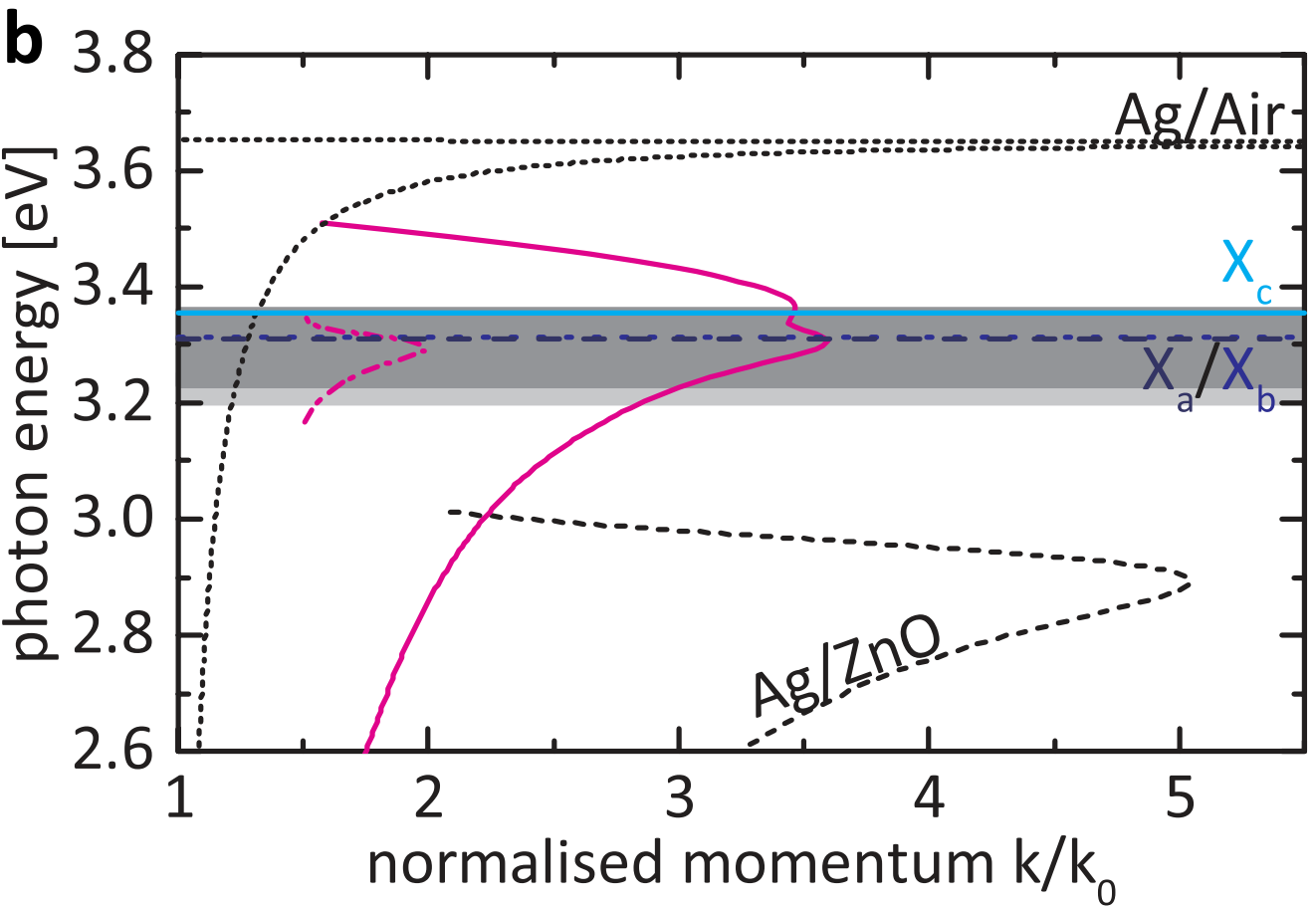
b
photon energy [eV]
3.8
3.6
3.4
3.2
3.0
2.8
2.6
1
2
3
4
5
normalised momentum k/k0
Ag/Air
Xc
Xa/Xb
Ag/ZnO

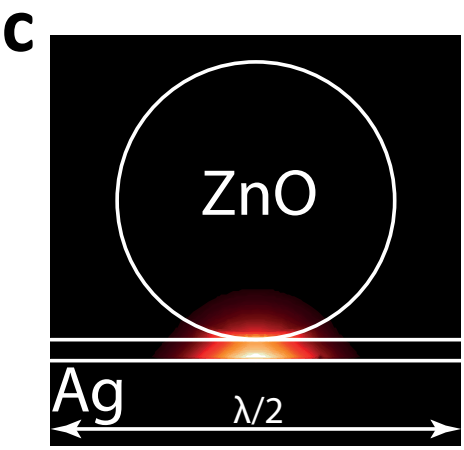
c
ZnO
Ag
λ/2

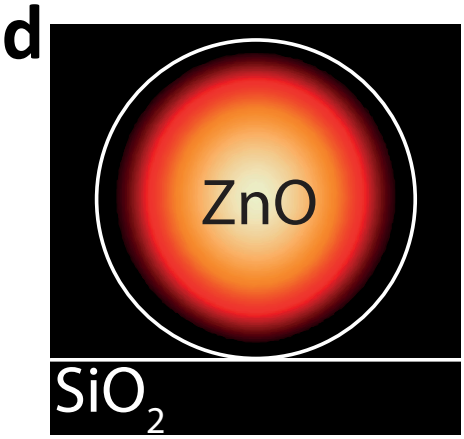
d
ZnO
SiO2

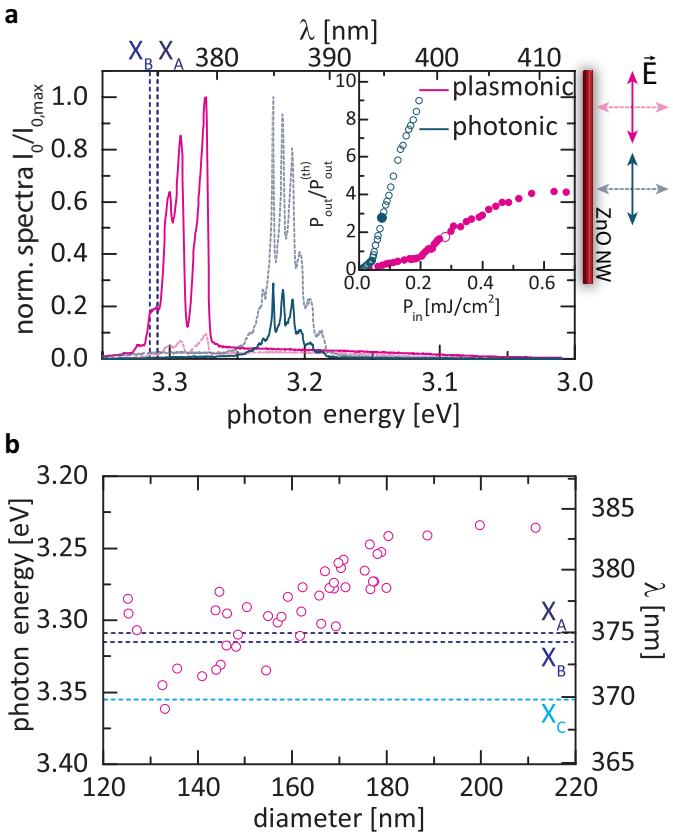
a
λ [nm]
X_B X_A
380
390
400
410
norm. spectra I_0/I_0,max
1.0
0.8
0.6
0.4
0.2
0.0
3.3
3.2
3.1
3.0
photon energy [eV]
plasmonic
photonic
P_out/P_out^(th)
10
8
6
4
2
0
0.0
0.2
0.4
0.6
P_in [mJ/cm²]
ZnO NW
E
b
photon energy [eV]
3.20
3.25
3.30
3.35
3.40
120
140
160
180
200
220
diameter [nm]
385
380
375
370
365
λ [nm]
X_A
X_B
X_C

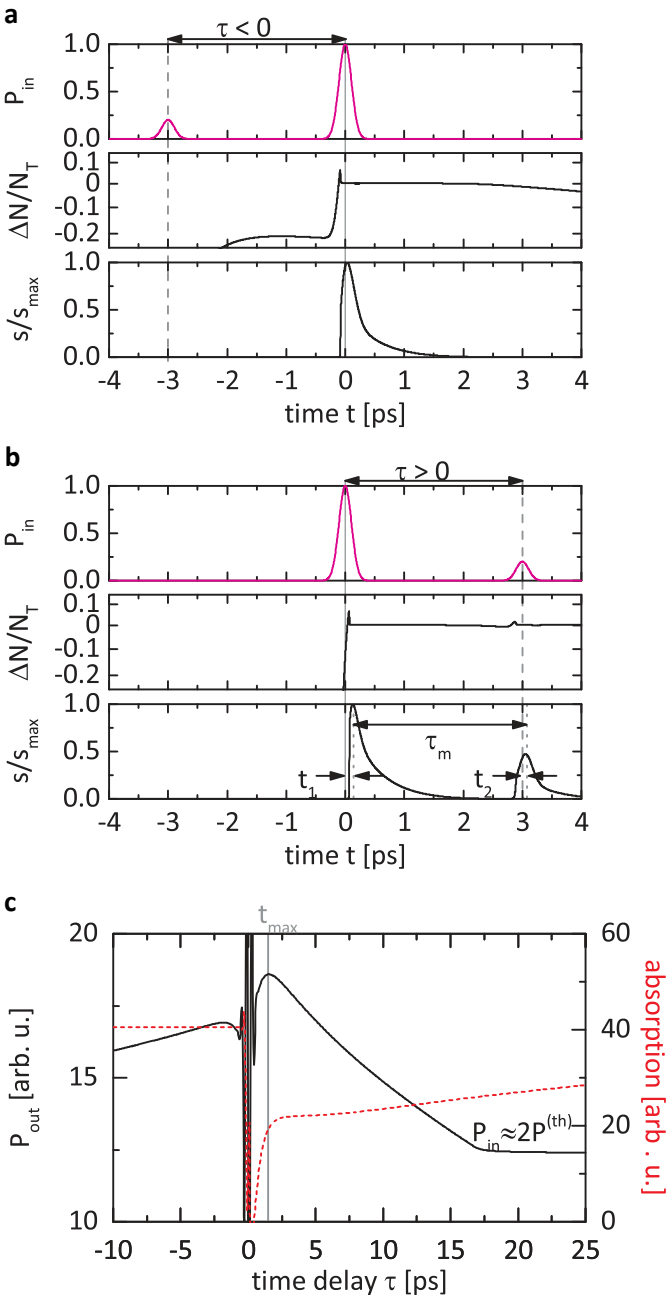
a
τ < 0
P_in
ΔN/N_T
s/s_max
time t [ps]
b
τ > 0
τ_m
t_1
t_2
time t [ps]
c
t_max
P_out [arb. u.]
absorption [arb . u.]
P_in≈2P^(th)
time delay τ [ps]

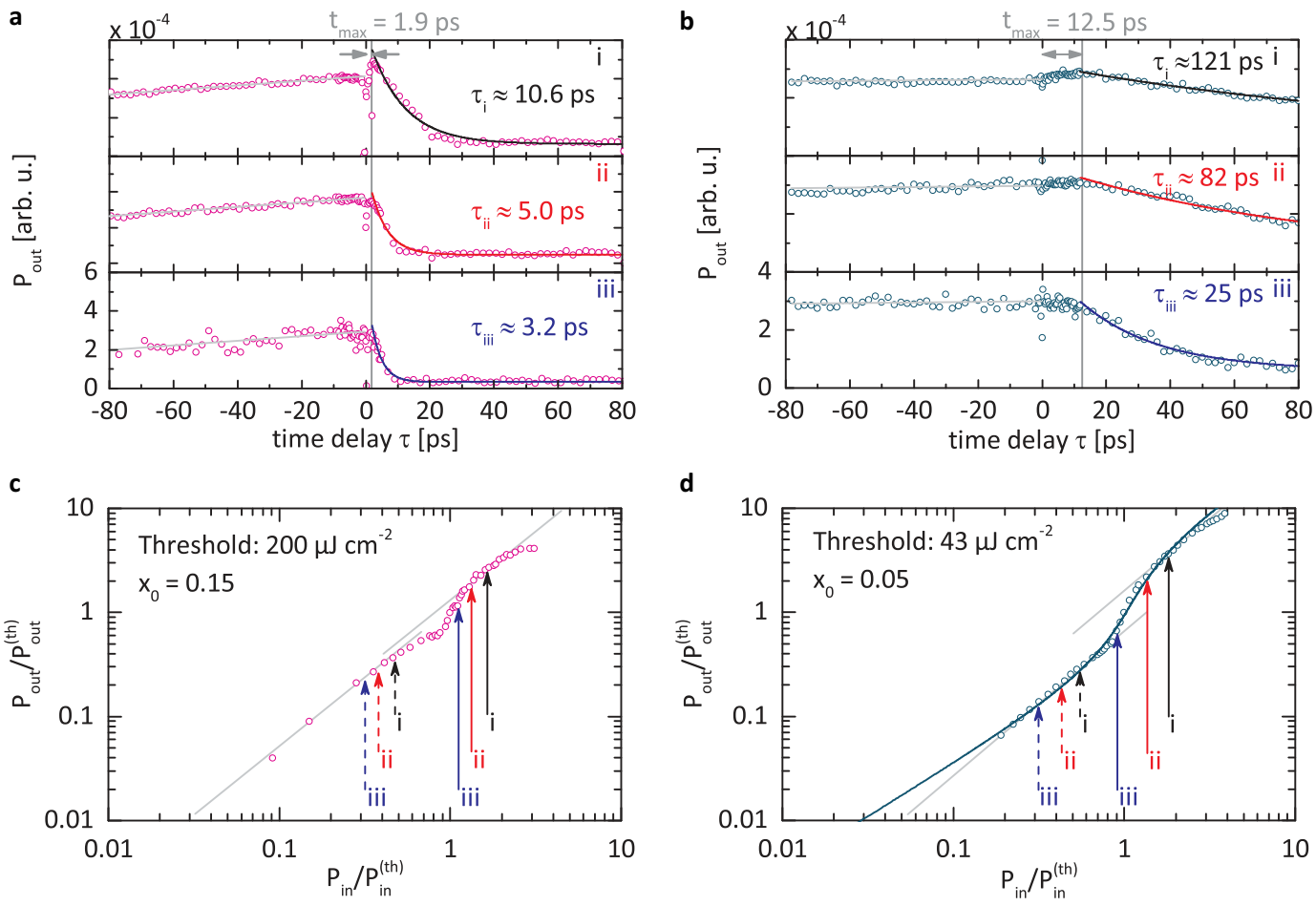
a
x 10^-4
t_max = 1.9 ps
τ_i ≈ 10.6 ps
τ_ii ≈ 5.0 ps
τ_iii ≈ 3.2 ps
i
ii
iii
P_out [arb. u.]
time delay τ [ps]
b
x 10^-4
t_max = 12.5 ps
τ_i ≈121 ps
τ_ii ≈ 82 ps
τ_iii ≈ 25 ps
P_out [arb. u.]
time delay τ [ps]
c
Threshold: 200 μJ cm^-2
x_0 = 0.15
P_out/P_out^(th)
P_in/P_in^(th)
d
Threshold: 43 μJ cm^-2
x_0 = 0.05
P_out/P_out^(th)
P_in/P_in^(th)

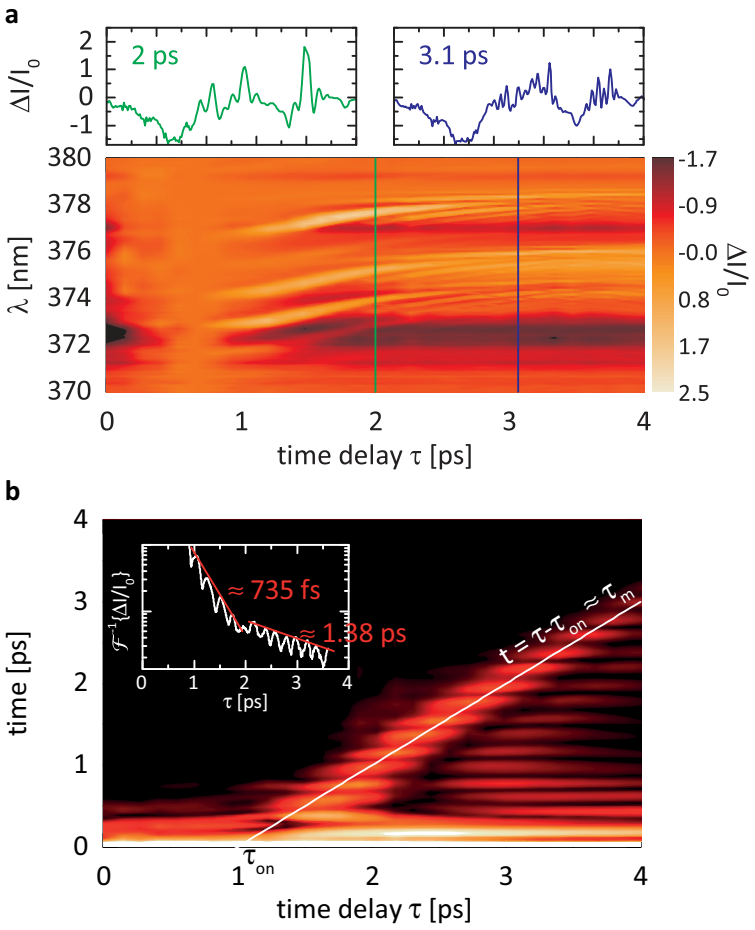
a
2 ps
3.1 ps
ΔI/I0
λ [nm]
time delay τ [ps]
b
time [ps]
≈ 735 fs
≈ 1.38 ps
τ [ps]
t = τ-τon ≈ τm
τon
time delay τ [ps]

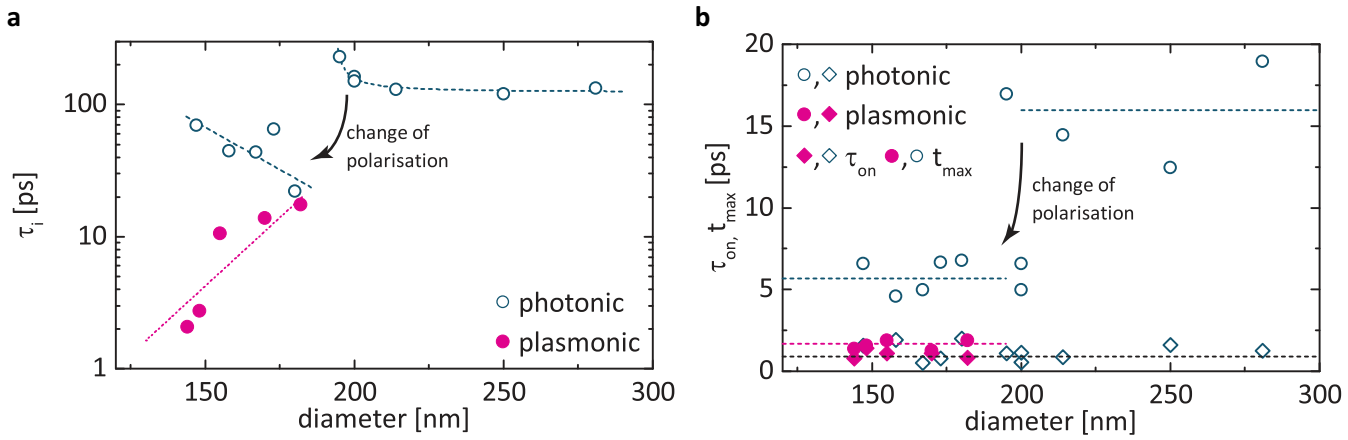
a
100
10
1
τ_i [ps]
150
200
250
300
diameter [nm]
change of
polarisation
photonic
plasmonic
b
20
15
10
5
0
τ_{on}, t_{max} [ps]
○,◇ photonic
●,◆ plasmonic
◆,◇ τ_{on} ●,○ t_{max}
change of
polarisation
150
200
250
300
diameter [nm]